Determining stress state of source media with identified difference between groundwater level during loading and unloading induced by earth tide

Huaizhong Yu (yuhz750216@sina.com)
China earthquake networks center
Chen Yu
China earthquake networks center
Binbin Zhao
Earthquake Agency of the Xinjiang Uygur Autonomous Region
Chong Yue
China earthquake networks center
Yulong Chang
Hunan Earthquake Agency

Research Article

Keywords: Groundwater level, Loading and unloading phases, Earth tide, Coulomb failure stress change, Dilatancy, Geodetic time series

Posted Date: April 21st, 2021

DOI: https://doi.org/10.21203/rs.3.rs-436988/v1

Determining stress state of source media with identified difference between groundwater level during loading and unloading induced by earth tide

Huaizhong Yu[1,*], Chen Yu[1], Binbin Zhao[2], Chong Yue[1], Yulong Chang[3]

1. China Earthquake Networks Center, Beijing 100045, China; yuchen@seis.ac.cn; yuechong@seis.ac.cn

2. Earthquake Agency of the Xinjiang Uygur Autonomous Region, Urumqi 830011, Xinjiang, China; tszhaobinbin@126.com

3. Hunan Earthquake Agency, Changsha 410004, Hunan, China; cyl@hundzj.gov.cn

* Correspondence: yuhz750216@sina.com; Tel.: +86-139-1006-2167

Abstract: The groundwater might be adopted as a useful tool to explore pre-seismic stress change in the crust, because it circulates in the deep crust and should be altered by the processes associated with the preparation of earthquakes. This work makes a new attempt that applies the load/unload response ratio (LURR) technique to study stress state of source media by calculating the ratio between water level during the loading and unloading phases. The change of Coulomb failure stress induced by earth tide in the tectonically preferred slip direction on the fault surface of the main shock is adopted for differentiating the loading and unloading periods. Using this approach, we test the groundwater level in the wells near the epicenters of some large earthquakes occurred in the Sichuan-Yunnan region of southwest China. Results show that the LURR time series fluctuate narrowly around 1.0 for many years, and climb to the maximum peaks prior to the main shocks. The magnitude of the pre-seismic peaks decreases with the distance from the epicenters. We hypothesized that the underlying physics of these changes might be explained by the pre-seismic dilatancy. The corresponding volume variations could be observed in the geodetic time series in the same neighborhoods.

Key words: Groundwater level; Loading and unloading phases; Earth tide; Coulomb failure stress change; Dilatancy; Geodetic time series.

1. Introduction

The instrumentally recorded data of groundwater level changes have been widely applied to study processes associated with occurrence of earthquakes, and reported in many literatures [1-3]. Roeloffs [4] revealed the response of water level changes in a well near the Parkfield to distant and local earthquakes. King et al. [5] detected the earthquake-related changes by analyzing co-seismic water level changes at 16 closely clustered wells with different depths. Brodsky et al. [6] suggested the mechanism of groundwater level changes and pressure induced by distant earthquakes. The results support the notion that observation of groundwater level changes helps us understand the responses of hydrogeologic system to earthquakes [7].

However, the exploration of the groundwater level changes before occurrence of earthquakes is much less. The reason might be that the current indexes of the anomalies for detection of the time, location and magnitude of future large earthquakes are mostly obtained

by using the statistical techniques [8], e.g. the groundwater level anomalies preceding the large earthquakes in China and Japan [9], the short-term pre-seismic changes in groundwater level in Turkmenistan [10], and the premonitory changes before the moderate local earthquakes and some large distant earthquakes in the well water level near the Tono mine in central Japan [11]. Due to the lack of understanding of the physical mechanism of earthquake preparation, less information can be extracted from the ambiguous anomalies and their uncertain time scales for the studies of earthquake potential [12-13].

In our latest studies [14], we find that the notion of Load/unload response ratio (LURR) may be applied to explore physical processes associated with the preparation of earthquakes via groundwater level. The LURR method is proposed by Yin et al. [15] and developed by Zhang et al. [16] and Yu et al. [17]. They believe that the variation of LURR time series is a proxy for the stress state of a heterogeneous brittle system (Fig. 1). When a nonlinear system is in the elastic phase, nearly the same responses (e.g., the strain, energy release and so on) to the loading and unloading are observed, and LURR ≈ 1.0; whereas when the system is stressed beyond the elastic limit, the responses become significantly different, and LURR > 1.0. Thus, the LURR value might be served as a useful parameter to assess criticality of earthquakes. Many publications have reported the anomalous enhancements prior to a large earthquake in the time series of LURR [18-20].

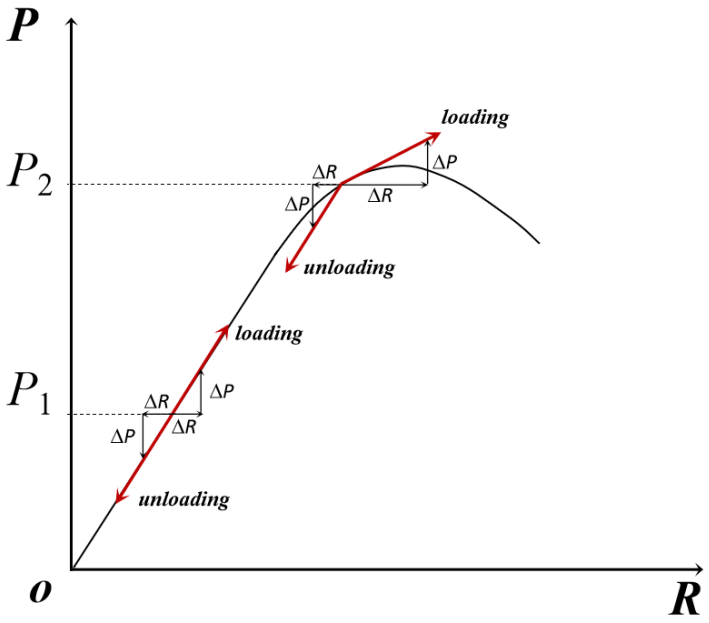

Figure 1. Schematic diagram of the constitutive relation of rock. P and R represent respectively the load and response. At the stage of P_1, the responses (ΔR) to the small changes of ΔP in the loading and unloading are almost the same, while at the stage of P_2, the response to the loading is significantly greater than the unloading.

Traditional LURR practice is based on the calculation of the ratio between Benioff strain releases during the time periods of loading and unloading, involving the evaluation of the Coulomb failure stress change [21] induced by earth tide and a regional earthquake catalog. Actually, recent studies have found that the tidal responses and earthquake-related changes can also be observed in the well water level [22]. The circulation of groundwater in the crust, especially in the fault zones, can reach 15 ~ 20 km, corresponding to the depth of most of earthquakes [23-24]. The small earthquakes or cracks result from the pre-seismic stress accumulation can cause rock dilatancy [25], and the magnified volume in the crust may lead to

the changes in groundwater level. If this were true, the groundwater level should be adopted as the loading/unloading response for calculation of LURR.

Based on this thought, in this study, we attempt to devise an approach to determine stress state of source media by applying the LURR method to identify the difference between groundwater level during the loading and unloading periods induced by earth tide. The method for differentiation of the loading and unloading phases follows the methodology of Coulomb failure stress change given by Yin et al. [26]. To show the validity of the approach, the groundwater level in the wells near the epicenters of the 2008 Ms8.0 Wenchuan, 2014 Ms6.5 Ludian, and 2019 Ms6.0 Changning earthquakes in the Sichuan and Yunnan provinces, southwest China are chosen as the examples.

2. Methods

Our approach is founded on the premise that the increased volume in rock result from the cracks generated by the establishment of criticality of an earthquake can change groundwater level in the nearby wells. Since cracks in rock are usually caused by shear stress [27], in our model, the Coulomb failure stress (*CFS*) induced by earth tide in the tectonically preferred slip direction on certain slip surface is used to determine stress change of source rock, and the Coulomb failure criterion is adopted to differentiate the loading and unloading phases (as Yin et al. [28] did in their LURR calculation using Benioff strain of small earthquakes as the loading/unloading response).

In the investigation of earthquake preparation, two stresses should be taken into consideration: the tidal and tectonic stresses [29]. The effective shear stress (τ_e) in earth crust is written as the common effect of the tectonic-effective shear stress ($\vec{\tau}_e^T$) and tidal-effective shear stress ($\vec{\tau}_e^t$):

$$\tau_e = \vec{\tau}_e^T + \vec{\tau}_e^t. \quad (1)$$

This shear stress is also called the *CFS* which is usually expressed as:

$$CFS = \tau - f\sigma, \quad (2)$$

where f, τ and σ denote respectively the inner frictional coefficient, shear stress and normal stress on the stress plane [30].

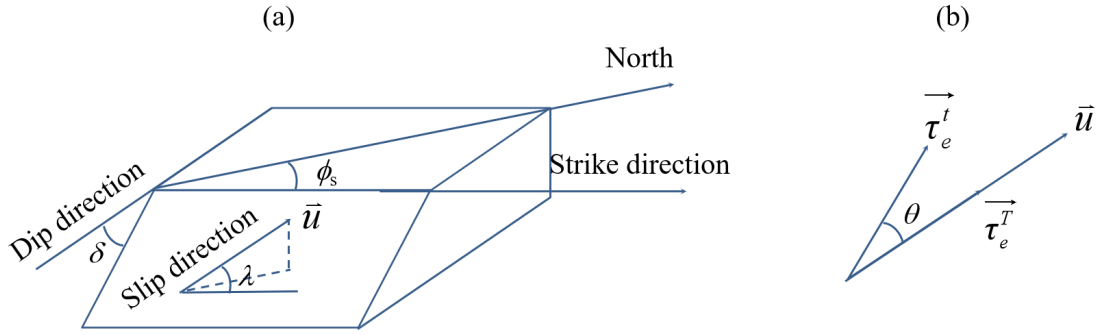

Figure 2. Schematic diagram of the determination of the loading and unloading induced by tidal stress. (a): the focal mechanism, (b): the relationship between the tectonic and tidal effective shear stresses. ϕ_s: fault strike, δ: dip angle, λ: slip direction, θ: angle between the tectonic and tidal effective shear stresses.

The orientation of tectonic-effective shear stress, which can be regarded as the principal stress orientation of *CFS* [31], is determined by the slip vector ($\vec{u}$) on the fault surface of the ensuing main shock [32]. $\vec{\tau}_e^T$ and $\vec{\tau}_e^t$ can then be defined as (Fig. 2a):

$$\vec{\tau}_e^T = \vec{\tau}^T - f\sigma^T \frac{\vec{u}}{|\vec{u}|}, \tag{3a}$$

$$\vec{\tau}_e^t = \vec{\tau}^t - f\sigma^t \frac{\vec{u}}{|\vec{u}|}. \tag{3b}$$

On the other hand, because the loading rate of tidal stress is much greater than the tectonic stress [29,33], i.e., $\frac{\Delta\tau_e^T}{\Delta t^T} \ll \frac{\Delta\tau_e^t}{\Delta t^t}$, the change of effective shear stress on the principal stress orientation can therefore be expressed as:

$$\Delta\tau_e = \vec{\tau}_e^t \cdot \frac{\vec{u}}{|\vec{u}|}. \tag{4}$$

Generally, the sign of $\Delta\tau_e$, which is decided by the angle of θ (Fig. 2b), determines the loading or unloading stressed by earth tide. When $\theta < \pi/2$, loading, and $\theta > \pi/2$, unloading.

If the rate of *CFS* is taken into consideration, the loading and unloading can then be decided by the sign of g which is defined as:

$$g = \frac{d}{dt}(\vec{\tau}_e^t \cdot \frac{\vec{u}}{|\vec{u}|}). \tag{5}$$

Following Eq. (5), the average values of groundwater level recorded in corresponding periods are adopted to compute LURR. Specifically,

$$Y = \frac{(\sum_{i=1}^{N+} H_i)/(N+)}{(\sum_{i=1}^{N-} H_i)/(N-)}, \tag{6}$$

where, *Hi* is groundwater level at the *i*-th record, and *N*+ or *N*- represent respectively the numbers of records during the loading and unloading periods. The time window used to calculate LURR values usually involves multiple load-unload cycles to reduce violent fluctuations in the curves.

Note that the method for calculation of tidal-induced stress is similar to the methodology proposed by Yin et al. [28]. The detailed algorithm has been listed by Yu et al. [34], in which the elastic deformation in crust induced by a celestial body is written as 6 differential equations of first order [35], and the stress components on any section can be derived by using the Runge-Kutta method [36].

3. Data preparation

The observation of groundwater level is subject to the monitoring instruments, artificial noise, and environmental influences, all of which cause errors of some kinds. Hence, the water level data are preprocessed by following procedures to enhance the quality for LURR calculation.

[1] To remove data extrema from the water level sequences. For the rock media, the magnitude of increased volume result from the cracks, in terms of the studies of Brace et al. [25], are no more than 2.0 times the elastic volume variations. Thus, the data points whose values exceed twice the average amplitude of water level sequence are removed.

[2] To linearly interpolate values to the missing data in the water level sequences.

[3] To perform 12 ~ 24 hours Butterworth band pass filtering on the data to remove signals unrelated to the tidal process.

4. Application to seismic data

As a retrospective study, we apply the LURR approach to the groundwater level in the wells near the epicenters of the M ≥ 6.0 earthquakes in the Sichuan-Yunnan region of southwest China. The study region is located geographically in the southeast Qinghai-Tibet plateau (Fig. 3). Because of the strong tectonic movement of Qinghai–Tibet plateau, the seismicity in this region is very active. The China Earthquake Administration (CEA) has monitored groundwater in this region for many years for seismic hazard evaluation. Nevertheless, there are only three earthquakes with suitable water level observations that can be applied to calculate LURR. They are: the May 12, 2008 Ms8.0 Wenchuan, August 3, 2014 Ms6.5 Ludian, and June 17, 2019 Ms6.0 Changning earthquakes.

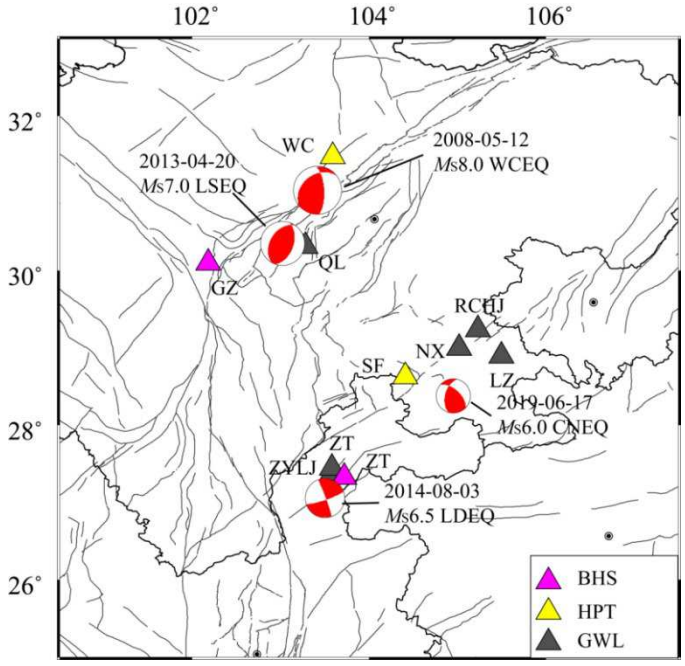

Figure 3. Location of selected earthquakes and corresponding observations. Four focal mechanisms, from big to small, represent the Wenchuan, Lushan, Ludian and Changning earthquakes. Triangles are location of the observation stations. BHS: borehole strain, HPT: Horizontal pendulum tiltmeter, and GWL: groundwater level. LZ: Luzhou, NX: Nanxi, QL: Qionglai, RCHJ: Rongchanghuajiang, SF: Shuifu, WC: Wenchuan, ZT: Zhaotong, ZYLJ: Zhaoyangleju, GZ: Guza.

Table 1. Detailed information of the well water level adopted for LURR calculation.

Event	Name of the wells	Epicentral distance (km)	Location of the wells (Lat/Lon)	Start time	Depth (m)	Sampling frequency
LDEQ	ZYLJ	35.8	27.38/103.58	20120524	114	1-hour
	ZT	42.8	27.45/103.58	20100101	350	1-hour
CNEQ	LZ	85	27.38/103.58	20130524	300	1-hour

	RCHJ	106	27.45/103.58	20140101	251	1-hour
	NX	71	28.98/104.93	20120601	105	1-hour
WCEQ	QL	76	30.32/103.28	20070630	175	1-hour

Note: The groundwater level observation at the NX well was stopped on April 1, 2019.

The groundwater level at 6 wells, in which the earth tide is observed clearly, were selected for calculation of LURR (Fig. 3). The distances from the ZYLJ and ZT wells to the epicenter of Ludian earthquake (LDEQ) are 35.8 and 42.8 km. Larger distances are from the QL well to the Wenchuan earthquake (WCEQ) (~76 km) and the NX, LZ and RCHJ wells to the Changning earthquake (CNEQ) (~71, 85 and 106 km). Tab. 1 lists the detailed information of the observation wells. The raw data of groundwater level were displayed in Fig. 4. The wells were installed from 2007 to 2014, whose depth goes from 100 to 400 meters. Fig. 5 shows some examples of the preprocessed water level data which are prepared for LURR calculation.

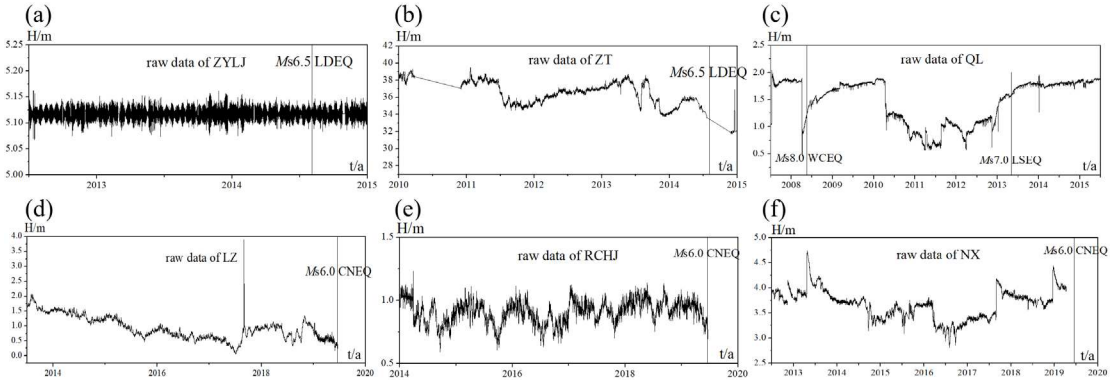

Figure 4. The raw data of groundwater level used for LURR calculation. The time of corresponding earthquakes in each of the maps is indicated by gray vertical lines.

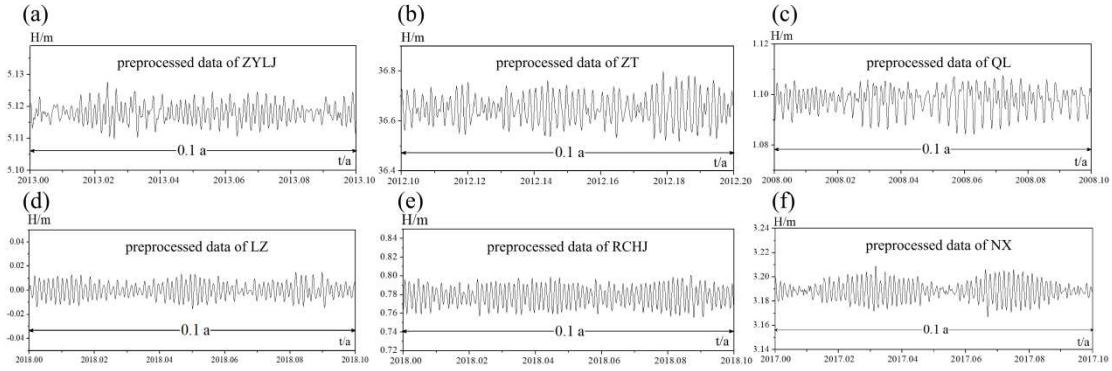

Figure 5. Examples of the filtered water level data.

Fig. 6 shows the time series of LURR produced using the groundwater level as data input, with the time window of 60 days at a sliding step of 30 days. Detailed source models and slip distributions (used for computing *CFS*) for the three main shocks are adopted from global CMT solution (http://www.globalcmt.org/), and the internal friction coefficient is 0.4 [28].

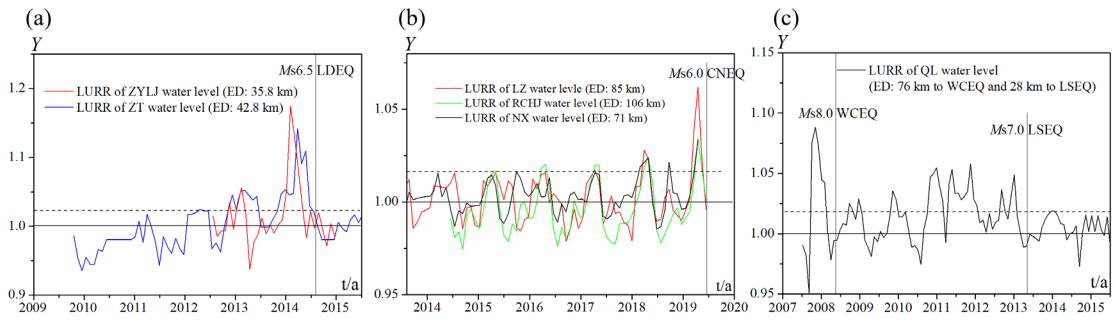

Figure 6. Time series of LURR produced with groundwater level in the wells shown in Fig. 3. The curves in (a), (b) and (c) are respectively for the LDEQ, CNEQ and WCEQ, with the time of the main shocks shown by gray vertical lines. The focal mechanism solutions adopted to calculate *CFS* are: LDEQ: strike=340, dip=86, slip=-9, depth=14, CNEQ: 207, 88, -177, 12, and WCEQ: 231, 35, 138, 13. ED: Epicentral distance.

5. Results and Interpretation

Comparing the LURR time series derived from the groundwater level at different wells, we find that significant anomalies can be observed prior to the ensuing large earthquakes. The LURR time series before the LDEQ began to increase at the end of 2012 and climbed to peaks in early 2014 (Fig. 6a), while the LURR peaked at the start of 2019 and end of 2007 for the CNEQ and WCEQ (Figs. 6b and 6c). The results could be supported by previous works of Yin et al. [28], which illustrated that the LURR evolve around 1.0 for many years until 1 ~ 2 years before the main shocks when, the LURR increase to the maxima (about 1.18, 1.07, and 1.09 for the three earthquakes), and subsequently return to a low level several months prior to the earthquakes.

On the other hand, there still are noticeable differences between the LURR curves:

[1] For the event with multiple observation wells, the magnitude of LURR anomalies decreases with the distance from the epicenter: the shorter the distance, the higher the peak. The LURR peak values prior to the LDEQ are 1.18 and 1.15 for the ZYLJ and ZT wells, while the corresponding distances from the epicenter are 35.8 and 42.8 km (Fig 6a). Similar scenarios can be observed in the LURR time series before the CNEQ (Fig. 6b).

[2] For some large events in the same neighborhoods, significant pre-seismic anomalies may also be detected not just to the target earthquake. As shown in Fig. 6c, in addition to the WCEQ in 2008, the LURR time series still yielded significant anomalies using the water level in the QL well before the 2013 Ms7.0 Lushan earthquake (LSEQ). The WCEQ and LSEQ ruptured respectively the northeastern and southern segments of Longmenshan fault zone (Fig. 3). The distance between two epicenters is just 86 km, and the QL well locate in the middle of them, with about 76 km to the WCEQ and 28 km to the LSEQ. Due to occurrence of the WCEQ, the increased stress on southern part of the Longmenshan fault [37] induced relatively high value of LURR until the LSEQ.

The evolution of LURR time series correlates well with the pre-seismic dilatancy suggested by Scholz et al. [38]. During this stage, the rock will become dilatant due to the generation of cracks, i.e., volume magnifies relative to the elastic variations [25]. Dilatancy begins to occur at relatively high level of stress, which alter water level in the near field wells by changing permeability and pressure. On the other hand, in terms of the Kaiser effect [39], the fracturing of rock during the loading and unloading periods is different under cyclical tide

stress. Since the cracks tend to occur in the loading rather than the unloading [40], the difference between water level during the loading and unloading periods is observed (Fig. 7).

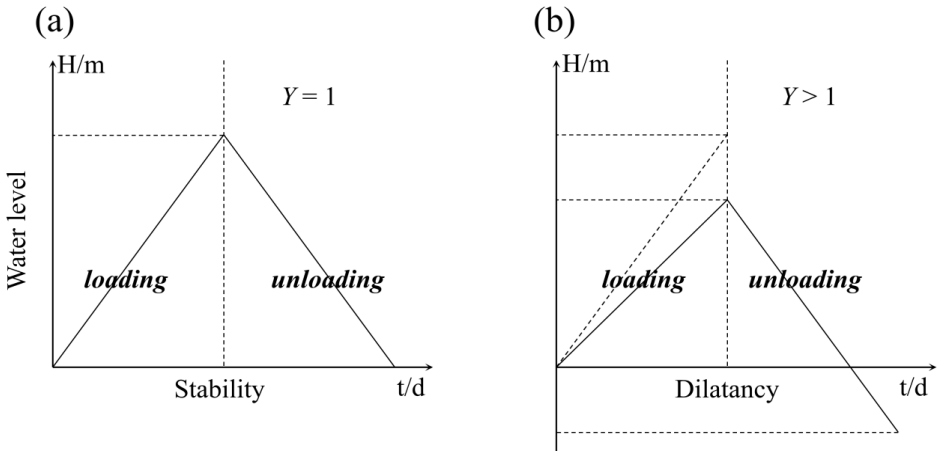

Figure 7. Schematic view of the influence of rock dilatancy on the water level and LURR. When the system is in the stable stage (a), there is no difference between water level during the loading and unloading phases, so $Y = 1$. When the system is in the dilatant stage (b), the void volume leads to the difference between water level during the loading and unloading. Because the void volume in the loading is far more than the unloading, the average water level in the loading is greater than the unloading, and $Y > 1$.

It is quite interesting that the stress state change in the crust identified by LURR may also be detected by the near field geodetic time series in the same time periods (Fig. 8). We found that the borehole strain (BHS) of ZT and GZ, and the horizontal pendulum tiltmeter (HPT) of SF and WC are about 49, 81, 57 and 56 km from the epicenters of the LDEQ, LSEQ, CNEQ and WCEQ (see Fig. 3). The marked compression in the ZT and GZ BHS in 2012 (Figs. 8a, b), obviously uplift changes in the SF HPT during 2018 ~ 2019 (Fig. 8c), and remarkable deflection in the WC HPT (Fig. 8d) provide potential evidences of volume variations for the pre-seismic dilatancy and its associated changes in the LURR time series produced using the near field well water level.

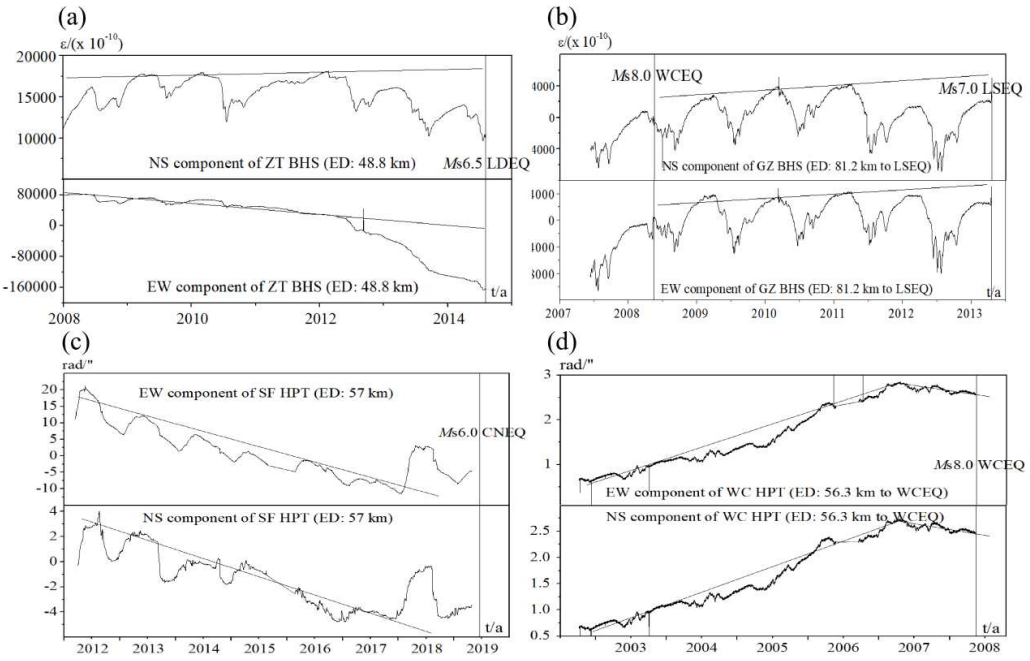

Figure 8. The geodetic time series observed near the LDEQ (a), LSEQ (b), CNEQ (c), and WCEQ (d). (a): the NS and EW components of the ZT BHS, (b): the NS and EW components of the GZ BHS, (c): the EW and NS components of the SF HPT, (d): the EW and NS components of the WC HPT.

6. Discussion

The LURR is a usable and convenient parameter for exploring crustal stress state. Compared with the raw data of groundwater level (Fig. 4), the pre-seismic changes identified by using the LURR technique look very significant in the entire sequence, which manifest the clearer warning signals for testing the final events. The LURR presented in this paper is evaluated based on the water level changes derived from the increased volume of cracks within the source rock. Since the tide stress is far less than the tectonic stress, cracks can only be triggered, not created, by tidal stress. When tectonic stress is at a low level (e.g., the elastic phase in Fig. 1), it is hard to induce any cracks by tidal stress. There was no noticeable difference between water level during the loading and unloading periods, so that $Y \approx 1.0$ (Fig. 7a). When tectonic stress reaches a relatively high level, the source rock is very sensitive to any tiny stress change, and cracks may therefore be triggered by the *CFS* result from tidal stress. Combined with the Kaiser effect, we note that cracks tend to be triggered by the increased *CFS*, i.e., under cyclical tide shear stress, more cracks occur during the loading than the unloading, resulting in the detectable difference in the groundwater level (Fig. 7b), and $Y > 1.0$.

The volume changes associated with the water level LURR anomalies could be found in the geodetic time series in the same neighborhoods. We note that the ZT BHS began to show marked compression in the mid-2012 (Fig. 8a), when the LURR values produced using the groundwater level of ZYLJ and ZT were greater than 1.02 (Fig. 6a). Similarly, the EW and NS components of the SF HPT (Fig. 8c) together with the LURR values derived from the LZ, NX and RCHJ wells began to increase in 2018 (Fig. 6b), while the time of LURR anomalies before the 2008 WCEQ (Fig. 6c) could be approved by the uplift changes in the EW and NS components of the WC HPT (Fig. 8d). A suitable explanation for the changes in the geodetic and LURR time series at almost the same time is the pre-seismic dilatancy [25]. The physical basis of the dilatancy model has been discussed by Wawersik and Brace [41]. Cracks increase

the void volume and change the stress state of source rock, so that the anomalous changes in the geodetic time series were observed, and then with influx of water, the increase of LURR values is observed.

In practice using the approach, when LURR is greater than a statistically critical value of Y^c, does tidal triggering of cracks occur. Our preliminary studies show that, for a $M \geq 6.0$ earthquake, the LURR have very significant efficiency when the epicentral distance is less than 100 km, and the efficiency decreases obviously when exceed this distance. When the system is far from the time of earthquake (the crustal system is running in a stable mode), the LURR value is basically less than 1.02 (indicated by the horizontal dashed lines shown in Fig. 6). When the system is close to the time of earthquake, the LURR is usually greater than 1.02, suggesting the establishment of criticality of earthquake. The LURR anomalies could last months to years and peaked right before the earthquake. Thus, 1.02 might be set as the optimally critical value of LURR for testing earthquakes in the Sichuan-Yunnan region.

Finally, the calculation of LURR requires relatively precise assessment of the direction of tectonic-effective shear stress which depends on the location and focal mechanism of ensuing large event [42]. For a given earthquake fault, if it is driven toward failure, its surrounding areas should be loaded to anomalously high level by the tectonic stress. The high stress state in areas surrounding the seismogenic fault is manifested by the sensitive changes of water level in the near field wells response to the cyclically tidal loading before the main shocks. Because the water level data are specially differentiated into the loading and unloading phases by using the effective shear change induced by the cyclical tide stress in the tectonically preferred slip direction on certain slip surface, rock dilatancy or development of cracks can be effectively identified, and the LURR anomalies for testing events in the same neighborhoods are therefore presented. Thus, where enough knowledge of active tectonics and stress setting exists, the LURR approach, combined with the high-quality water level observations, can be tuned toward detecting the regional stress state and potential risk of future large earthquakes.

7. Conclusion

We find that by calculating the ratio between groundwater level during the loading and unloading periods induced by tidal stress, marked changes might be detected prior to occurrence of large earthquakes. The anomalous changes have certain significance for prediction of future earthquakes. For a $M \geq 6.0$ earthquake in the Sichuan-Yunnan region, the critical LURR value is about 1.02 and the anomalies can last several months to years. The changes could be attributed to the pre-seismic dilatancy, with the volume changes in earth crust detected by the geodetic time series in the same neighborhoods. Combination of the pre-seismic changes in the LURR and geodetic time series would represent less ambiguous alarms for ensuing large earthquakes. At present time, the application of this method for real-time prediction of earthquake must be approached with caution because the pre-determined source models are needed. Nevertheless, the attempts shown in this paper make us to systematically search for the time and location of various kinds of earthquakes by using the near-field water level, if sufficient knowledge of regional tectonic stress setting are known. More importantly, our approach elucidates an important feature of groundwater level that could be combined with the physically feasible models for seismic hazard evaluation.

Author Contributions: H.Y. wrote the main manuscript text, C.Y. prepared figures 1-2, B.Z. and Y.C. prepared figures 3-6 and Table 1, C.Y. prepared figures 7-8. All authors reviewed the manuscript.

Acknowledgments: We thank the China Earthquake Networks Center for providing groundwater level and crustal deformation data. All the data are archived and available in the Mendeley data repository (https://data.mendeley.com/datasets/5zhjhb6ftp/1). This work has been supported by the Earthquake

Joint Funds of NSFC (Grant No. U2039205) and the National Key Research and Development Project (Grant No. 2018YFE0109700).

Conflicts of Interest: The authors declare no conflict of interest.

References

[1] Koizumi, N.; Kitagawa, Y.; Matsumoto, N.; Takahashi, M.; Sato, T.; Kamigaichi, O.; Nakamura, K. Pre-seismic groundwater level changes induced by crustal deformations related to earthquake swarms off the east coast of Izu Peninsula, Japan, Geophys Res Lett, **2004**, 31, L10606.

[2] Wang, C.; Manga M. Earthquakes and Water, Springer Berlin Heidelberg, **2010**.

[3] Yuce, G.; Ugurluoglu, D.Y.; Adar, N.; Yalcin, T.; Yaltirak, C.; Streil, T.; Oeser, V. Monitoring of earthquake precursors by multi-parameter stations in Eskisehir region (Turkey), Applied Geochemistry, **2010**, 25 (4), 572-580.

[4] Roeloffs, E.A. Persistent water level changes in a well near Parkfield, California, due to local and distant earthquakes, J. Geophys. Res., **1998**, 103 (B1), 869-889.

[5] King, C.Y.; Azuma, S.; Igarashi, G.; Ohno, M.; Saito, H.; Wakita, H. Earthquake related water level changes at 16 closely clustered wells in Tono, central Japan, J. Geophys. Res., **1999**, 104 (B6), 13073-13082.

[6] Brodsky, E.E.; Roeloffs, E.; Woodcock, D.; Gall, I.; Manga, M. A mechanism for sustained groundwater pressure changes induced by distant earthquakes, J. Geophys. Res., **2003**, 108 (B8), 2390.

[7] Montgomery, D.R.; Manga, M. Streamflow and water well response to earthquake, Science, **2003**, 300, 2047-2049.

[8] Cicerone, R.D.; Ebel, J.E.; Britton, J. A systematic compilation of earthquake precursors, Tectonophysics, **2009**, 476, 371-396.

[9] Roeloffs, E.A. Hydrologic precursors to earthquakes: A review, Pure Appl. Geophys., **1988**, 126 (2), 177-209.

[10] Kissin, I.G.; Belikov, V.M.; Ishankuliev, G.A. Short-term groundwater level variations in a seismic region as an indicator of the geodynamic regime, Tectonophysics, **1996**, 265, 313-326.

[11] King, C.Y.; Azuma, S.; Ohno, M.; Wakita, H. In search of earthquake precursors in the water-level data of 16 closely clustered wells at Tono, Japan, Geophysical Journal International, **2008**, 143 (2), 469-477.

[12] Liu, Y.W.; Chen, T.; Xie, F.R.; Du, F.; Yang, D.X.; Zhang, L.; Xu, L.Q. Analysis of fluid induced aftershocks following the 2008 Wenchuan Ms 8.0 earthquake, Tectonophysics, **2014**, 149, 619-620.

[13] Skelton, A.; Andrén, M.; Kristmannsdóttir, H.; Stockmann, G., et al. Changes in groundwater chemistry before two consecutive earthquakes in Iceland, Nature Geoscience, **2014**, 7, 752-756.

[14] Ma, Z.; Yu, C.; Zhang, X.T.; Yu, H.Z. Evolutions of LURR Anomaly based on Seismicity and Groundwater Level Data before the June 17, 2019 M6.0 Changning Earthquake, Earthquake Research in China, **2020**, 36 (3), 550-560 (In Chinese with English abstract).

[15] Yin, X.C.; Chen, X.Z.; Song, Z.P.; Yin C. A New Approach to Earthquake Prediction–The Load/Unload Response Ratio (LURR) Theory, Pure Appl. Geophys., **1995**, 145, 701-715.

[16] Zhang, Y.X.; Yin, X.C.; Peng, K.Y. Spatial and Temporal Variation of LURR and its Implication for the Tendency of Earthquake Occurrence in Southern California, Pure Appl. Geophys., **2004**, 161, 2359-2367.

[17] Yu, H.Z.; Zhou, F.R.; Cheng, J.; Wan, Y.G. The sensitivity of loa/unload response ratio and critical region selection before large earthquakes, Pure Appl. Geophys., **2015**, 172 (8), 173-183.

[18] Yu, H.Z.; Shen, Z.K.; Wan, Y.G.; Zhu, Q.Y.; Yin, X.C. Increasing critical sensitivity of the Load/Unload Response Ratio before large earthquakes with identified stress accumulation pattern, Tectonophysics, **2006**, 428 (1-4), 87-94.

[19] Yu, H.Z.; Zhu, Q.Y. A Probabilistic Approach for Earthquake Potential Evaluation Based On the Load/Unload Response Ratio Method, Concurrency and Computation: Practice and Experience, **2010**. 22, 1520-1533.

[20] Liu, Y.; Yin X.C. A dimensional analysis method for improved load-unload response ratio, Pure Appl. Geophys., **2018**, 175 (2), 633-645.

[21] Jaeger, J.C.; Cook, N.G.W. Fundamentals of Rock Mechanics, Chapman and Hall, London, **1976**. 78-99.

[22] Igarashi, G.; Wakita, H. Tidal responses and earthquake-related changes in the water level of deep wells, J. Geophys. Res., **1991**, 96, 4269-4278.

[23] Muir-Wood, R.; King G. Hydrological signatures associated with earthquakes train, J. Geophys. Res., **1993**, 98 (12), 22035-22068.

[24] Gudmundsson, A.; Berg, S.; LysloK, B. Fracture networks and fluid transport in active fault zone, Journal of Structure Geology, **2001**, 23 (2), 343-353.

[25] Brace, W.B.; Paulding, J.R.; Scholz, C. Dilatancy in the fracture of crystalline rocks, J. Geophys. Res., **1966**, 71 (16), 3939-3953.

[26] Yin, X.C.; Zhang, L.P.; Zhang, Y.X.; Peng, K.Y.; Wang, H.T.; Song, Z.P.; Yu, H.Z. The newest developments of load-unload response ratio (LURR), Pure Appl. Geophys., **2008**, 165, 711- 722.

[27] Byerlee, J.D. Friction of rocks, Pure Appl. Geophys., **1978**, 116, 615 - 626.

[28] Yin, X.C.; Wang, Y.C.; Peng, K.; Bai, Y.L.; Wang, H.; Yin, X.F. Development of a New Approach to Earthquake Prediction: Load/Unload Response Ratio (LURR) Theory, Pure Appl. Geophys., **2000**, 157, 2365-2383.

[29] Harris, R.A. Earthquake stress trigger, stress shadows, and seismic hazard, J. Geophys. Res., **1998**, 103, 24347-24358.

[30] Zoback, M.D.; Zoback, M.L.; Mount, V.; Wentworth, C.M. New evidence on state of stress of the San Andreas fault system, Science, **1987**, 238, 1105-1111.

[31] Emter, D. Tidal triggering of earthquakes and volcanic events, Helmut, et al., eds., Tidal phenomena, Springer, **1997**, 293-309.

[32] Hardebeck, J.L.; Hauksson, E. Crustal stress field in southern California and its implications for fault mechanics. J. Geophys. Res., **2001**, 106, 21859-21882.

[33] Vidali, J.E.; Agnew, D.C.; Johnston, M.J.S.; Oppenheimer, D.H. Absence of earthquake correlation with earth tides: an indication of high preseismic fault stress rate, J. Geophys. Res., **1998**, 103, 24567-24572.

[34] Yu, H.Z.; Yu, C.; Ma, Z.; Zhang, X.T.; Zhang, H.; Yao, Q.; Zhu, Q.Y. Temporal and spatial evolution of load/unload response ratio before the M7.0 Jiuzhaigou earthquake occurred on Aug. 8, 2017 in Sichuan Province, Pure Appl. Geophys., **2020**, 177, 321-331.

[35] Dziewonski, A.M.; Anderson, D.L. Preliminary reference earth model, Physics of the Earth and Planetary Interiors, **1981**, 25, 297-356.

[36] Melchior, P. The Tide of the Planet Earth, Pergamon Press, New York, **1978**.

[37] Pei, S.P.; Niu, F.L.; Ben-zion, Y.; Sun, Q.; Liu, Y.B.; Xue, X.T.; Su, J.R.; Shao, Z.G. Seismic velocity reduction and accelerated recovery due to earthquakes on the Longmenshan fault, Nature Geoscience, **2019**, 12, 680.

[38] Scholz, C.H.; Sykes, L.R.; Aggarwal, Y.P. Earthquake prediction: A physical basis, Science, **1973**, 181, 803-809.

[39] Li, C.; Nordlund, E. Experimental verification of the Kaiser effect in rocks, Rock Mech Rock Engng, **1993**, 26 (4), 333-351.

[40] Kurita, K.; Fujii, N. Stress memory of crystalline rocks in acoustic emission, Geophys Res Lett, **1979**.6, 9-12.

[41] Wawersik, W.R.; Brace, W.F. Post-failure behavior of a granite and diabase, Rock Mechanics, **1971**, 3 (2), 61-85.

[42] Hauksson, E.L.; Jones, M.; Hutton, K. The 1999 Mw7.1 Hector Mine, California, earthquake sequence: Complex conjugate strike-slip faulting, Bull. Seism. Soc. Am., **2002**, 92, 1154-1170.

Figures

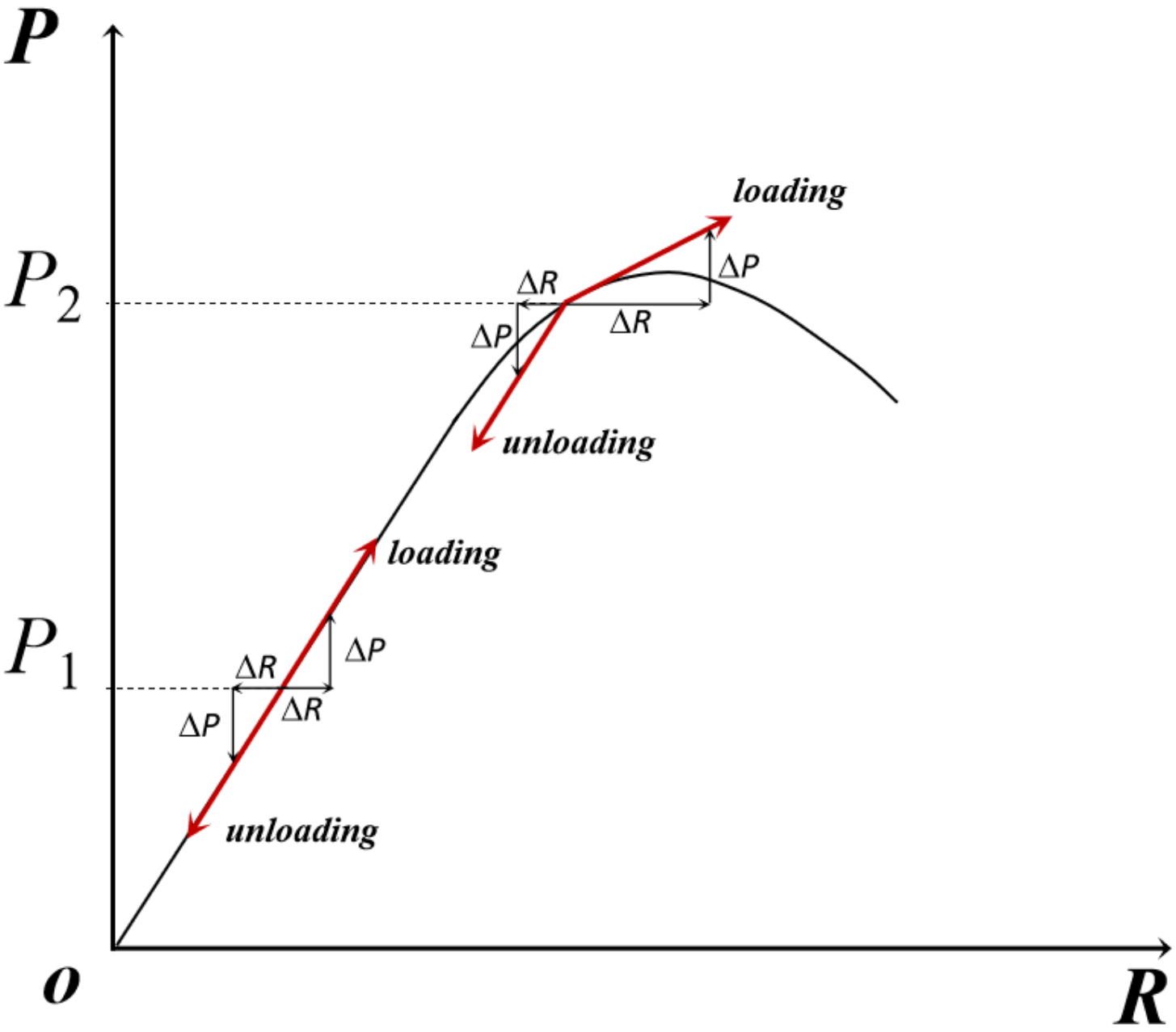

Figure 1

Schematic diagram of the constitutive relation of rock. P and R represent respectively the load and response. At the stage of P1, the responses (DR) to the small changes of ΔP in the loading and unloading are almost the same, while at the stage of P2, the response to the loading is significantly greater than the unloading.

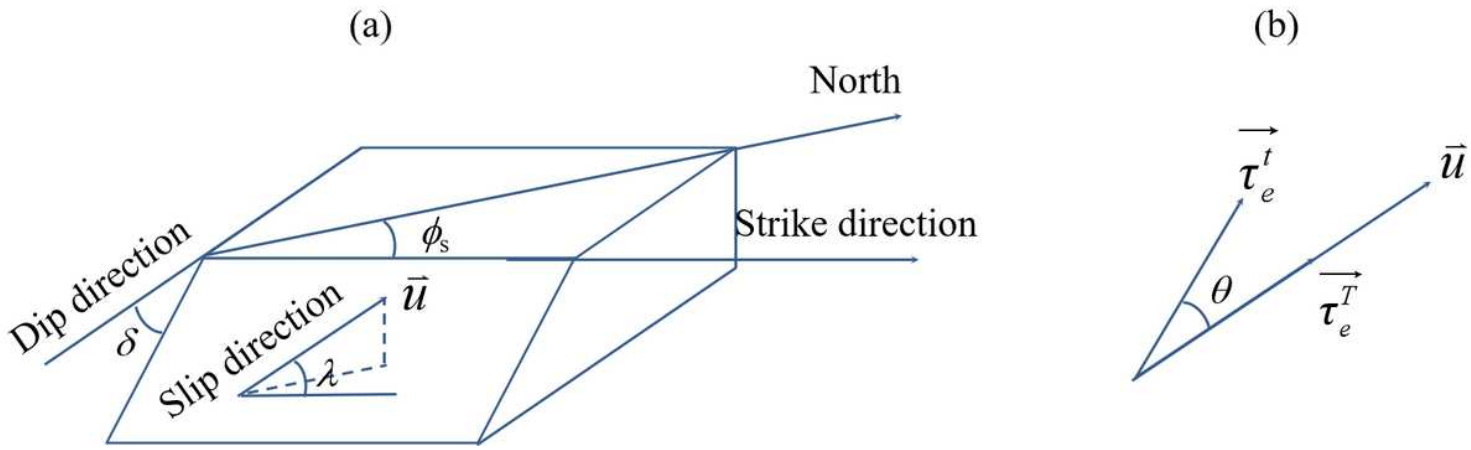

Figure 2

Due to technical limitations, the caption for this figure is only available in the manuscript file.

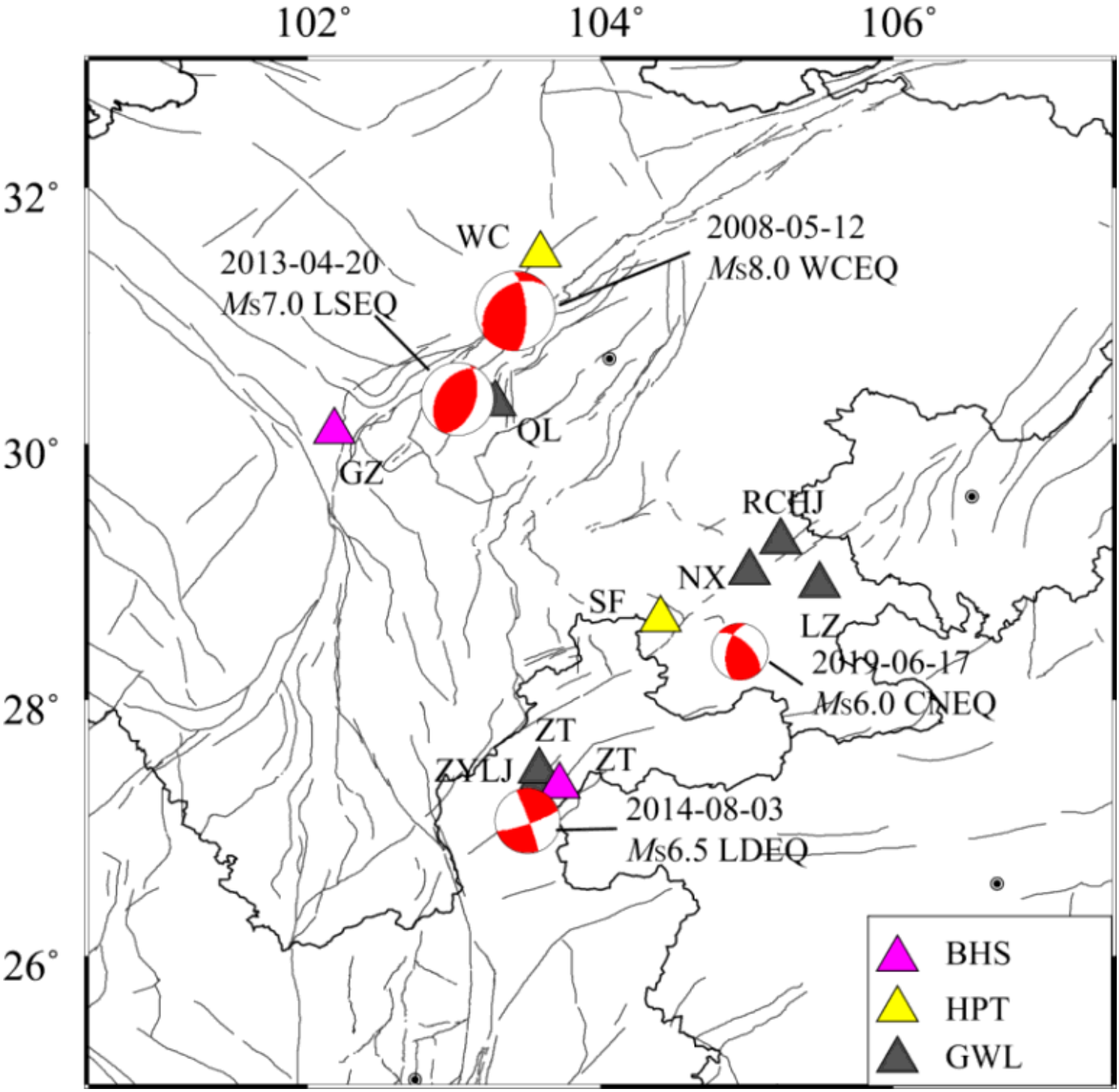

Figure 3

Location of selected earthquakes and corresponding observations. Four focal mechanisms, from big to small, represent the Wenchuan, Lushan, Ludian and Changning earthquakes. Triangles are location of the observation stations. BHS: borehole strain, HPT: Horizontal pendulum tiltmeter, and GWL: groundwater level. LZ: Luzhou, NX: Nanxi, QL: Qionglai, RCHJ: Rongchanghuajiang, SF: Shuifu, WC: Wenchuan, ZT: Zhaotong, ZYLJ: Zhaoyangleju, GZ: Guza. Note: The designations employed and the presentation of the material on this map do not imply the expression of any opinion whatsoever on the part of Research

Square concerning the legal status of any country, territory, city or area or of its authorities, or concerning the delimitation of its frontiers or boundaries. This map has been provided by the authors.

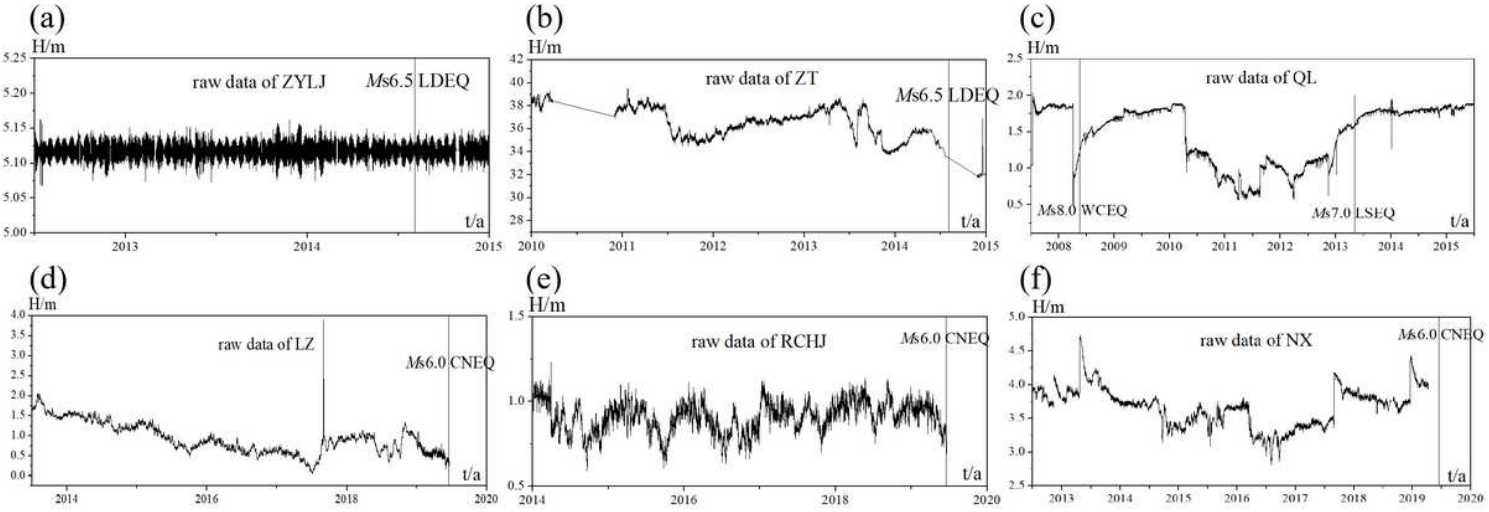

Figure 4

The raw data of groundwater level used for LURR calculation. The time of corresponding earthquakes in each of the maps is indicated by gray vertical lines.

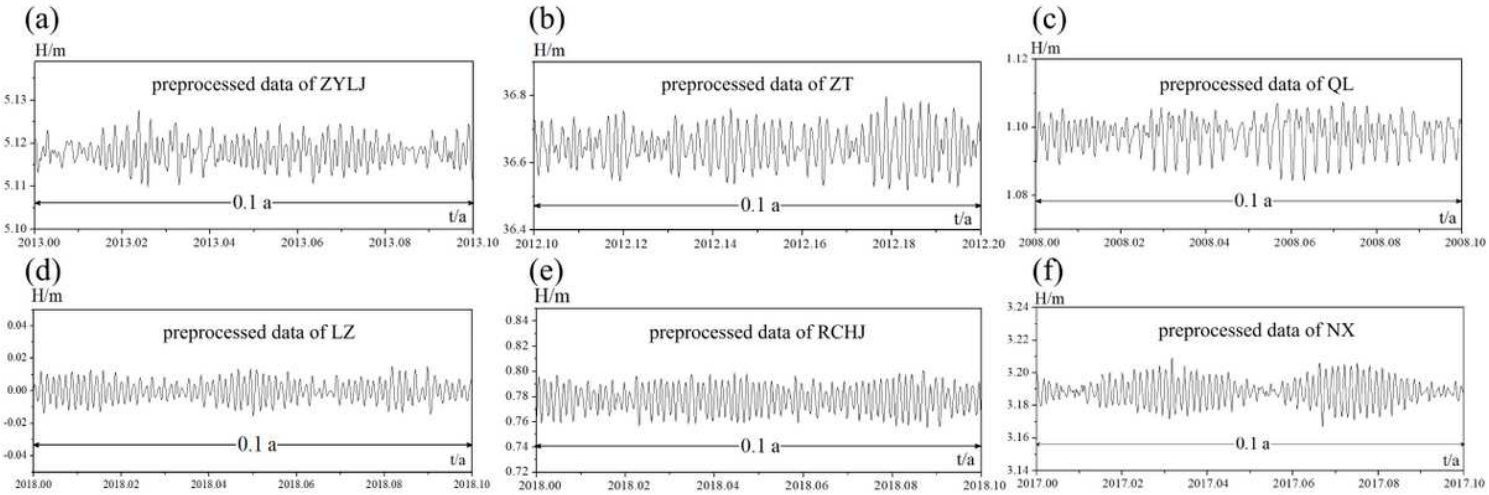

Figure 5

Examples of the filtered water level data.

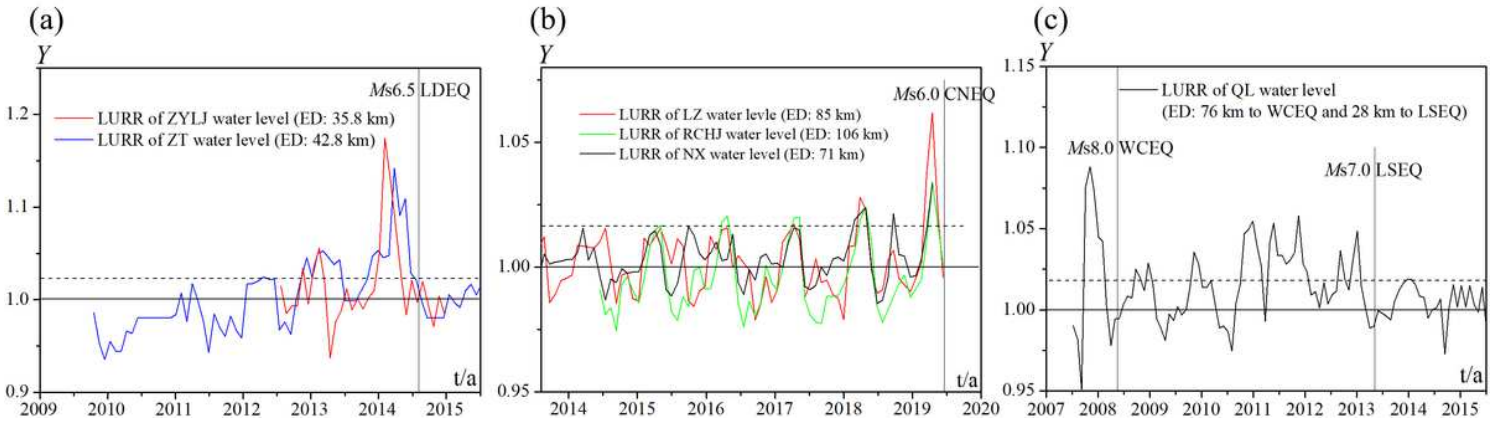

Figure 6

Time series of LURR produced with groundwater level in the wells shown in Fig. 3. The curves in (a), (b) and (c) are respectively for the LDEQ, CNEQ and WCEQ, with the time of the main shocks shown by gray vertical lines. The focal mechanism solutions adopted to calculate CFS are: LDEQ: strike=340, dip=86, slip=-9, depth=14, CNEQ: 207, 88, -177, 12, and WCEQ: 231, 35, 138, 13. ED: Epicentral distance.

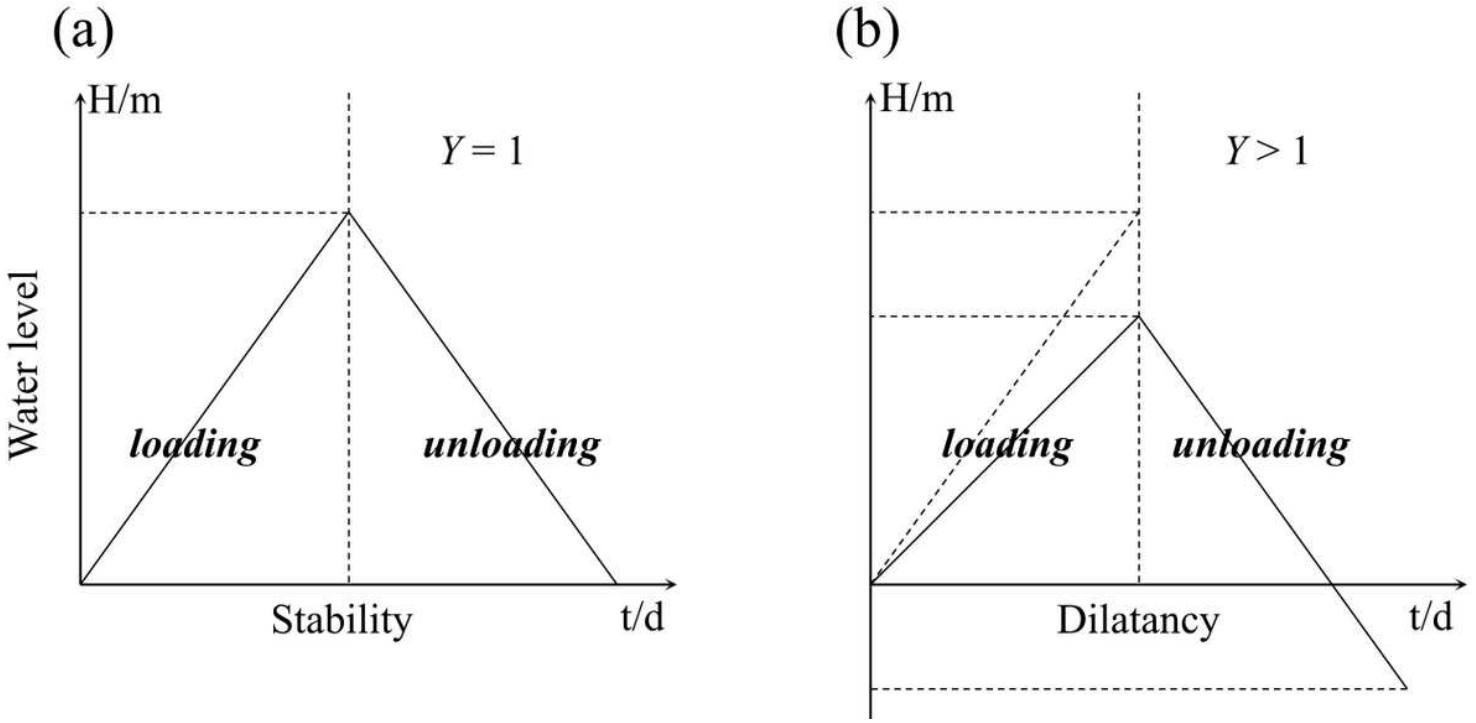

Figure 7

Schematic view of the influence of rock dilatancy on the water level and LURR. When the system is in the stable stage (a), there is no difference between water level during the loading and unloading phases, so Y = 1. When the system is in the dilatant stage (b), the void volume leads to the difference between water level during the loading and unloading. Because the void volume in the loading is far more than the unloading, the average water level in the loading is greater than the unloading, and Y > 1.

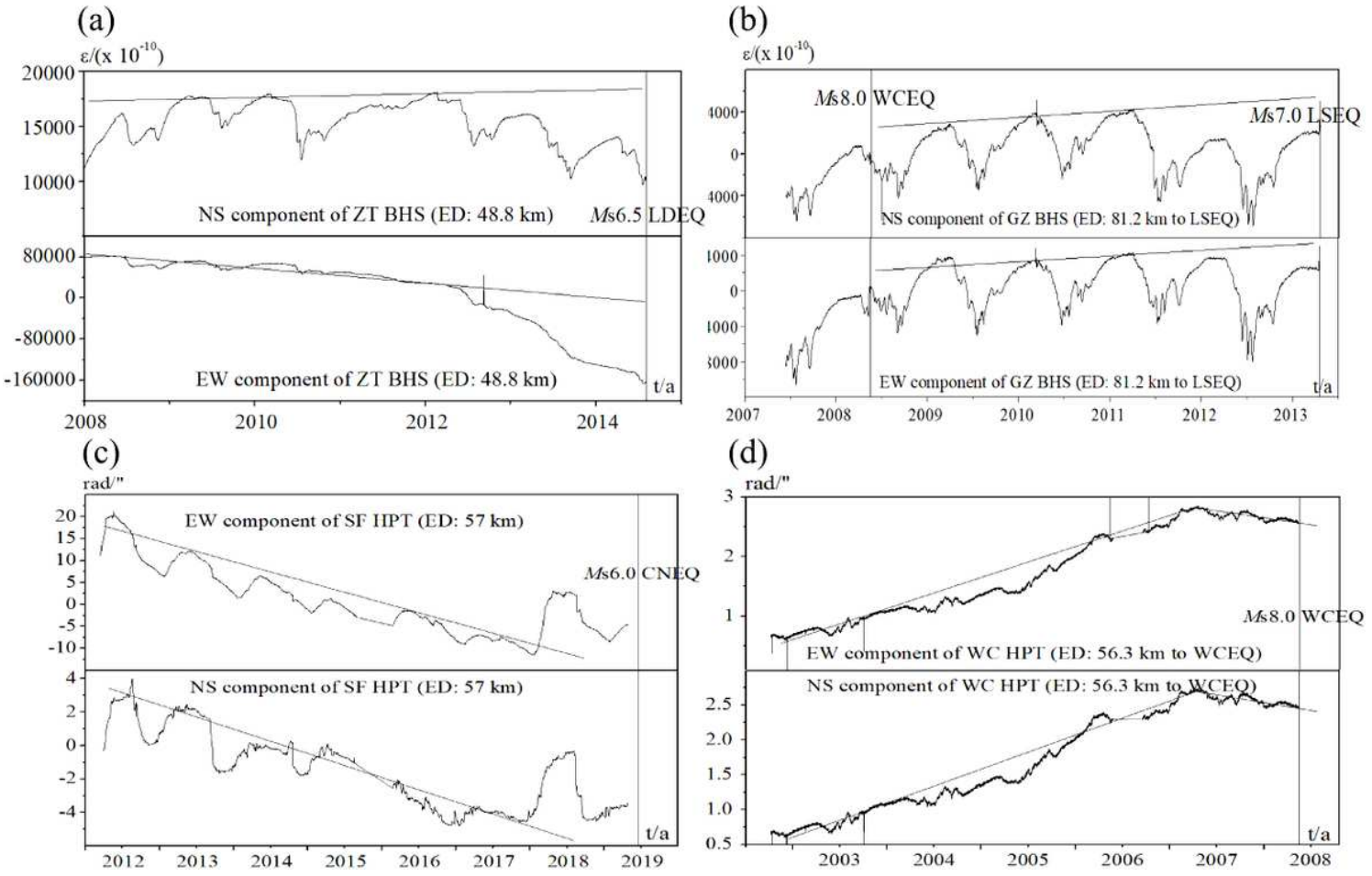

Figure 8

The geodetic time series observed near the LDEQ (a), LSEQ (b), CNEQ (c), and WCEQ (d). (a): the NS and EW components of the ZT BHS, (b): the NS and EW components of the GZ BHS, (c): the EW and NS components of the SF HPT, (d): the EW and NS components of the WC HPT.